Supplemental Information

Active Regulation of Receptor Ratios Controls Integration of Quorum Sensing Signals in *Vibrio harveyi*

Table of Contents

A. Supporting Measurements

A.1. Measuring AI-1 Production by Wild-type LuxM and a LuxM-GFP Translational Fusion

To measure the levels of LuxM protein, we used a translational fusion of full-length LuxM to GFP. We tested the functionality of the LuxM-GFP fusion as follows. A 1:128 dilution of cell-free culture fluids from *E. coli* carrying plasmids expressing wild-type LuxM, LuxM-GFP, or an empty vector were applied to the *V. harveyi* AI-1 sensing strain, TL25. Light production from the reporter strain was subsequently measured. We found no significant difference between AI-1 production from the LuxM-GFP fusion and wild-type LuxM.

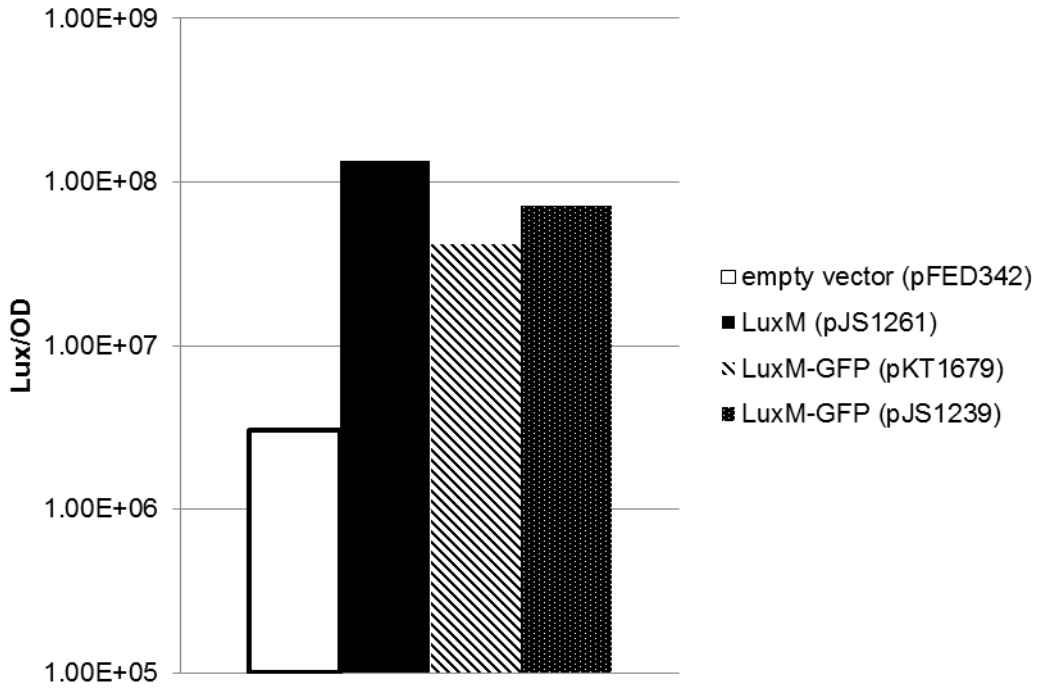

Figure S1. Comparison of a LuxM-GFP fusion with WT LuxM. AI-1 production by various LuxM proteins was measured as follows. *E. coli* strains bearing the indicated plasmids were grown overnight in LB medium containing the appropriate antibiotic at 37^{o}C. Cultures were

diulted 1:100, and grown for approximately 4 h. Cell free culture fluids were collected, diluted 1:128 and applied to the AI-1 sensor strain *V. harveyi* TL25. Prior to application, TL25 was grown overnight in AB medium at 30^{o}C and diluted 1:10,000 into fresh AB medium containing 1mM boric acid. 10% cell-free culture fluids from the LuxM producing *E. coli* strains were applied to the reporter strain. Light production and OD_{600} were monitored using a 96-well plate reader.

A.2. LuxN-FLAG Functionality in WT *V. harveyi*

The LuxN-FLAG construct used in these studies was inserted on the *V. harveyi* chromosome and was thus the only copy of LuxN present in particular strains. To verify LuxN-FLAG functionality, we tested the ability of LuxN-FLAG to respond to AI-1 using a bioluminescence assay (Freeman et al, 2000). Indeed, the LuxN-FLAG construct behaved like wild type LuxN

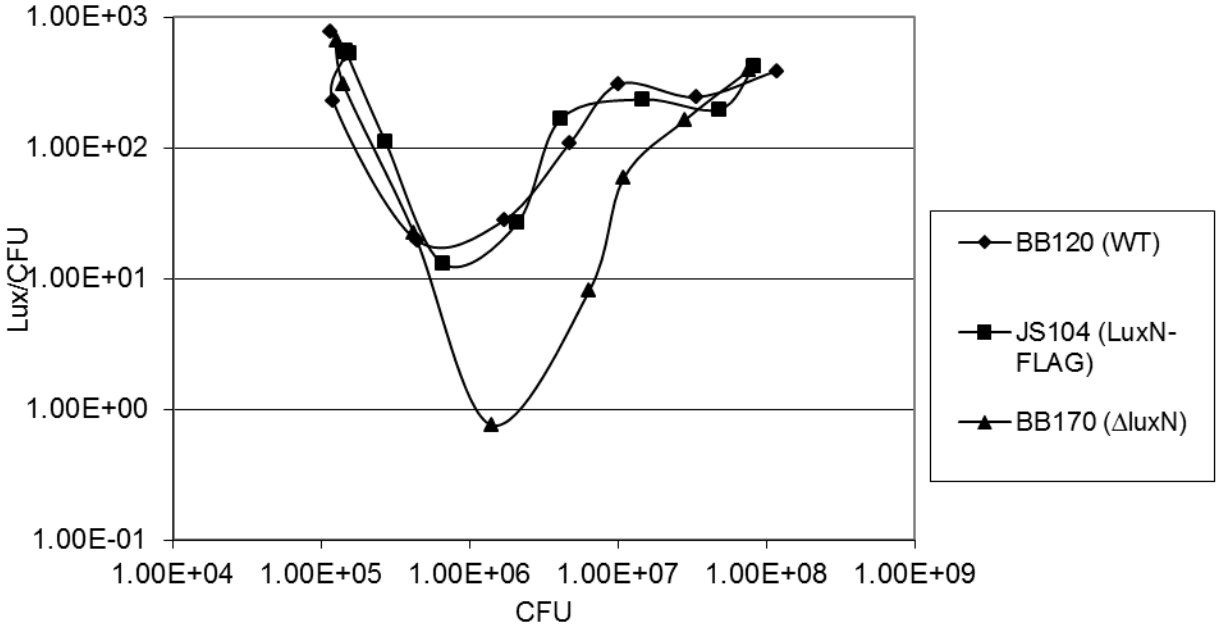

Figure S2. Response of *V. harveyi* strains to AI-1. Strains were grown overnight in AB medium and then diluted 1:5000 into fresh AB medium containing 10% cell-free culture fluids collected from a Δ*luxS V. harveyi* strain. Bioluminescence and cell density were monitored, and the resulting Lux/CFU was plotted against CFU.

A.3. LuxR-mCherry Functionality in WT Loop Strain

To demonstrate that the LuxR-mCherry protein fusion is functional, we measured expression of *gfp* driven by a LuxR-controlled promoter (P_{CMW275}) on the chromosome (Waters and Bassler, 2005) in the WT Loop strain. We compared the input-output relation between AI and P_{CMW275}-GFP for the LuxR-mCherry strain (Figure S3A) and a wild-type LuxR strain (Figure S3B). The color contours are rescaled by the minimum and maximum fluorescence output of each strain. The overall shapes of the input-output relations for two strains are similar, although the repression by LuxR-mCherry is roughly two-fold reduced compared to wild-type LuxR. As expected, the input-output contours in Figure S3 are anti-correlated with LuxR levels in Figure 4B. We conclude that the LuxR-mCherry fusion used in our studies is functional, although the fusion modestly affects the repression strength. The fact that *gfp* expression differs by 2-fold when LuxR is at its lowest level suggests that fusion of mCherry to LuxR increases the strength of LuxR repression of its targets. We suspect that the LuxR-mCherry protein binds more strongly to DNA than does wild-type LuxR.

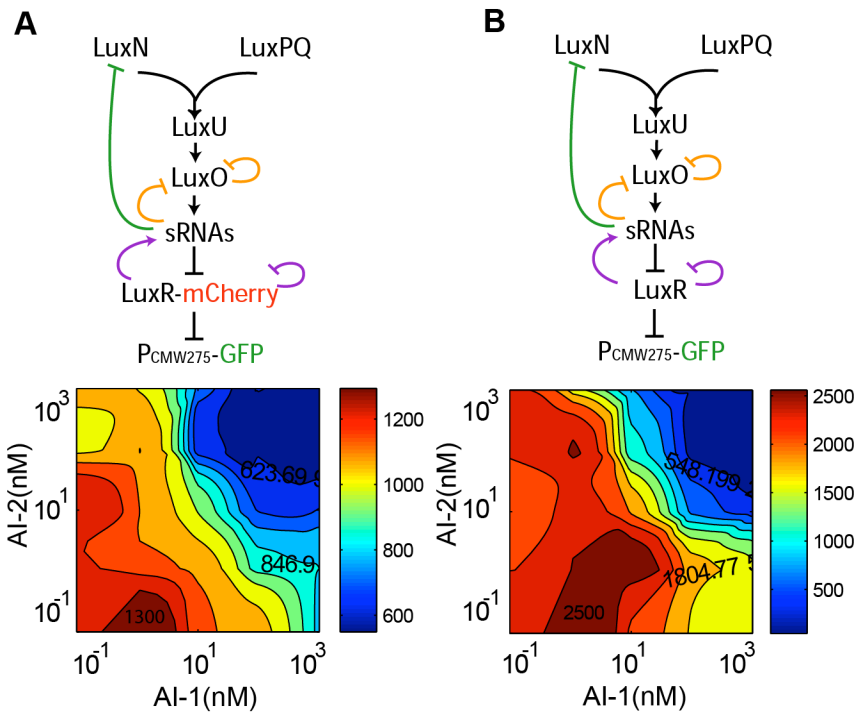

Figure S3. Comparison of repression by LuxR-mCherry and wild-type LuxR. We compared the expression level of *gfp* driven by a LuxR-repressed promoter (P_{CMW275}) on the chromosome as a function of the concentrations of AI-1 and AI-2. (The numerical scale is in A.U., and the contour colors are rescaled by the minimum and maximum fluorescence output of each strain.). (A) GFP is repressed by LuxR-mCherry. (B) GFP is repressed by wild-type LuxR.

A.4. LuxR Loop Construction and Functionality

To construct the LuxR loop mutation, we engineered a missense mutation into LuxR (R17C) that does not affect transcription of *luxR* mRNA but renders LuxR incapable of DNA binding (Hammer and Bassler, 2003; Svenningsen et al., 2008). To demonstrate that LuxR (R17C)-mCherry cannot activate gene expression, we measured bioluminescence in strains carrying LuxR-mCherry and LuxR (R17C)-mCherry fusions in a Δ*luxR* background (Figure S4). The

results show that no light is produced when LuxR (R17C)-mCherry is present indicating that LuxR (R17C)-mCherry is incapable of gene regulation.

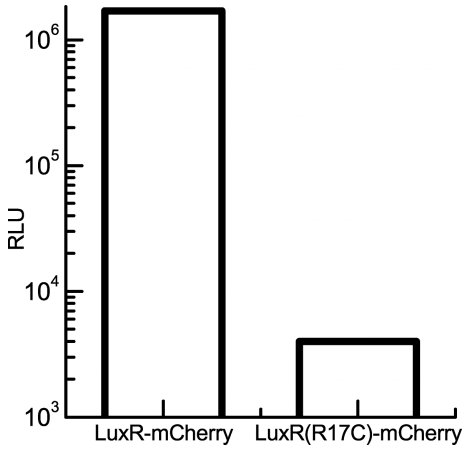

Figure S4. Functionality of wild-type LuxR and LuxR (R17C). Bioluminescence output in the presence of wild-type LuxR or LuxR (R17C).

A.5. LuxN Protein Expression Level and LuxN-mCherry Functionality

To directly measure LuxN protein levels, we fused mCherry to LuxN via a C-terminal fusion on the chromosome in the WT Loop *V. harveyi* strain. We found that LuxN-mCherry retains functionality by comparing expression of the quorum-sensing-activated luciferase operon in the presence of wild-type LuxN (left) or LuxN-mCherry (right) for four different AI input conditions in our WT strain that is Δ*luxM*, Δ*luxS*, Δ*cqsS* (Figure S5A). Light production for [AI-1] = 1μM is many-fold higher than for [AI-1] = 0, irrespective of whether AI-2 is present or absent, indicating that the LuxN-mCherry construct is functional.

We measured the LuxN protein levels by measuring LuxN-mCherry expression using single-cell fluorescence microscopy for four different AI concentrations (Figure S5B). A strong increase in LuxN protein level occurs with increasing AI concentrations. The relative LuxN protein expression levels are similar to the *luxN* mRNA expression levels in Figure 6A.

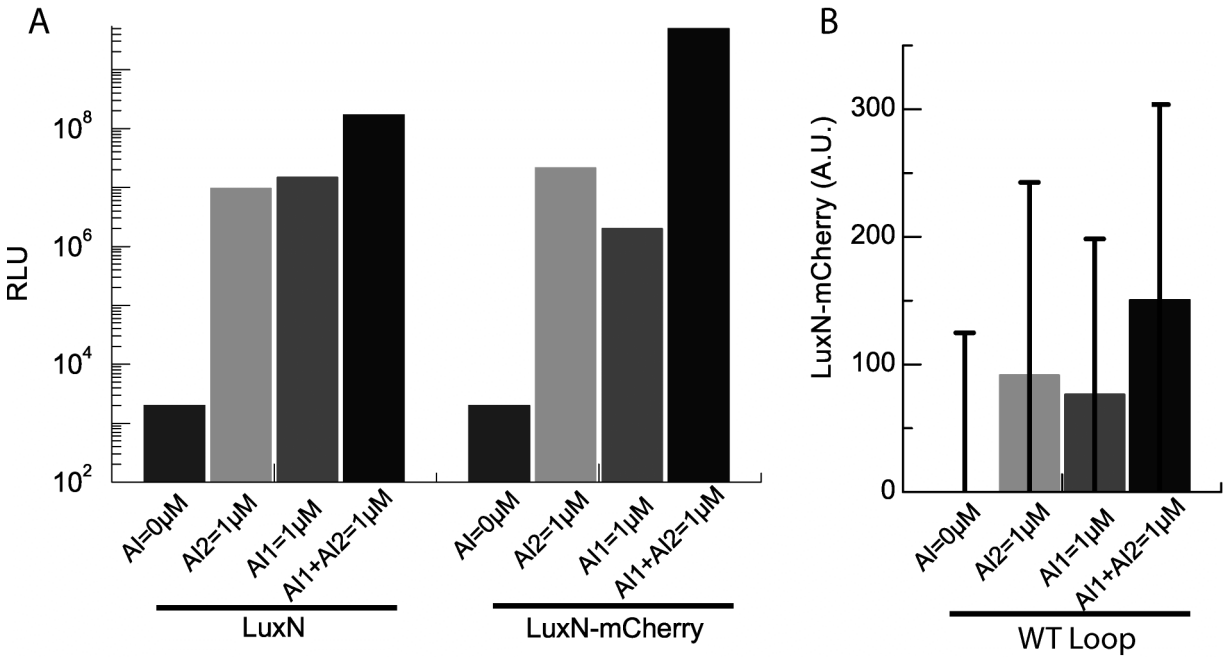

Figure S5. Functionality and expression level of LuxN-mCherry.

(A) Bioluminescence output of the quorum-sensing-activated luciferase operon in the presence of LuxN and LuxN-mCherry at four different AI concentrations. The LuxN-mCherry fusion responds to AI-1. (B) LuxN-mCherry levels at four different AI concentrations. (Due to the low copy number of LuxN, we significantly increased the exposure time for this figure. For this reason, the fluorescence intensity is in arbitrary units).

A.6. LuxN-on Strain Construction and Supporting Measurements

To construct the WT LuxN-on (ST165) and the LuxOLoop LuxN-on (ST168) strains, we deleted the *luxN* gene from the chromosome by allelic recombination in the WT Loop and LuxO Loop mutant strain using pST153 carrying Δ*luxN*::Cm^r. We eliminated the antibiotic resistance marker on the chromosome to generate the WT Loop Δ*luxN* (ST161) strain and the LuxOLoop Δ*luxN* (ST163) mutant. Figure S4 shows the mean LuxR contour for the WT Loop Δ*luxN* strain

carrying an empty vector pJV025 containing Kan^r. The figure demonstrates that the WT Loop Δ*luxN* strain does not respond to AI-1 (bottom edge of Figure S6B).

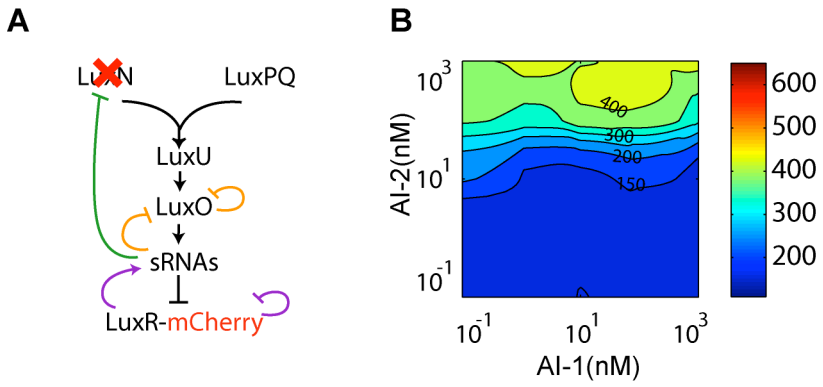

Figure S6. The mean LuxR contour of the WT Loop Δ*luxN* **strain.** (A) The quorum-sensing circuit of the WT Loop Δ*luxN* strain. (B) The mean LuxR contour plot for this strain.

We constructed plasmid pST157 containing IPTG and Theophyline inducible *luxN*-Kan^r derived from pJV025 template. We introduced pST157 into KT833 and KT836 to make the ST165 and ST168 strains. We found that the maximum inducer concentration in which the strains grow normally was IPTG = 10μM and Theophyline = 1μM. We measured LuxR-mCherry levels in the WTLoop LuxN-on strain (Figure S7A) and the LuxOLoop LuxN-on strain (Figure S7B) at different AI and inducer concentrations. No difference in response to AI-1 occurred between zero inducer (left) and full inducer (right) suggesting that the construct is leaky and the basal level of LuxN production in the absence of inducers is high enough to give a saturating AI-1 signal response. For this reason, we did not use the IPTG or Theophyline inducers in our studies (Figure 6).

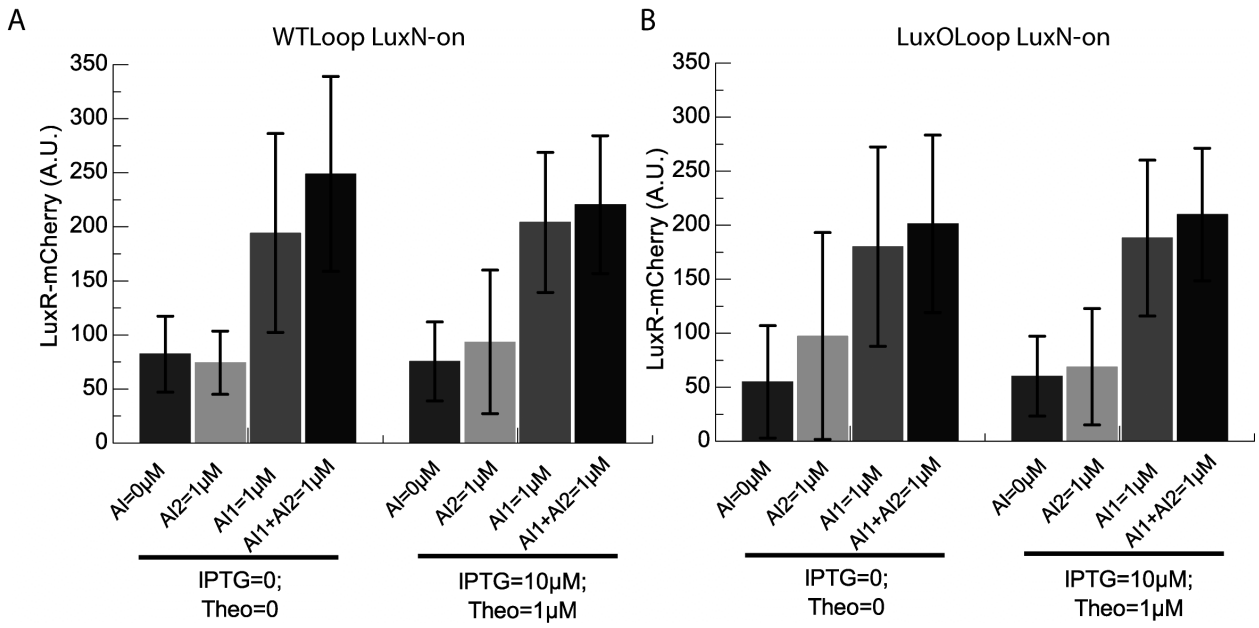

Figure S7. Comparison of LuxR expression in the WT LuxN-on and LuxOLoop LuxN-on strains. (A) The WT LuxN-on strain without inducer (left panel) and under full inducer (IPTG = 10μM and Theophyline = 1μM) (right panel) conditions. (B) The LuxOLoop LuxN-on strain under no inducer (left panel) and in full inducer (IPTG = 10μM and Theophyline = 1μM) (right panel) conditions.

A.7. Interpolation for the input-output relationship and day-to-day variation.

The 3D bar-plot of WT Loop strain (Figure S8A) illustrates the raw data of Figure 4B with no interpolation. The major features of the input-output relation in Figure S8A remain the same as in Figure 4B. As such, the interpolation algorithm does not affect the interpretation of the input-output contour. (Source data for Figure 4 is available at http://www.nature.com/msb.) Furthermore, data from a duplicate experiment (Figure S8B) is similar to that in Figure S8A, demonstrating that day-to-day variation is minor.

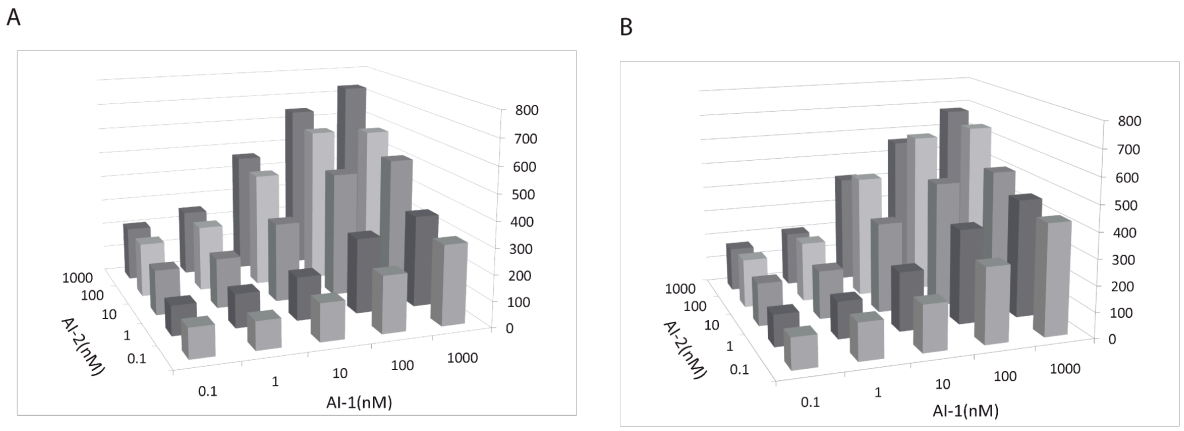

Figure S8. 3D bar plot of WT Loop *V. harveyi* strain. (A) Mean LuxR copy number as a function of AI-1 and AI-2 concentrations. (B) Biological duplicate obtained under the same biological conditions with the same experimental prepartaion as in (A). We reproduced the same

experiment in order to show the day-to-day variation.

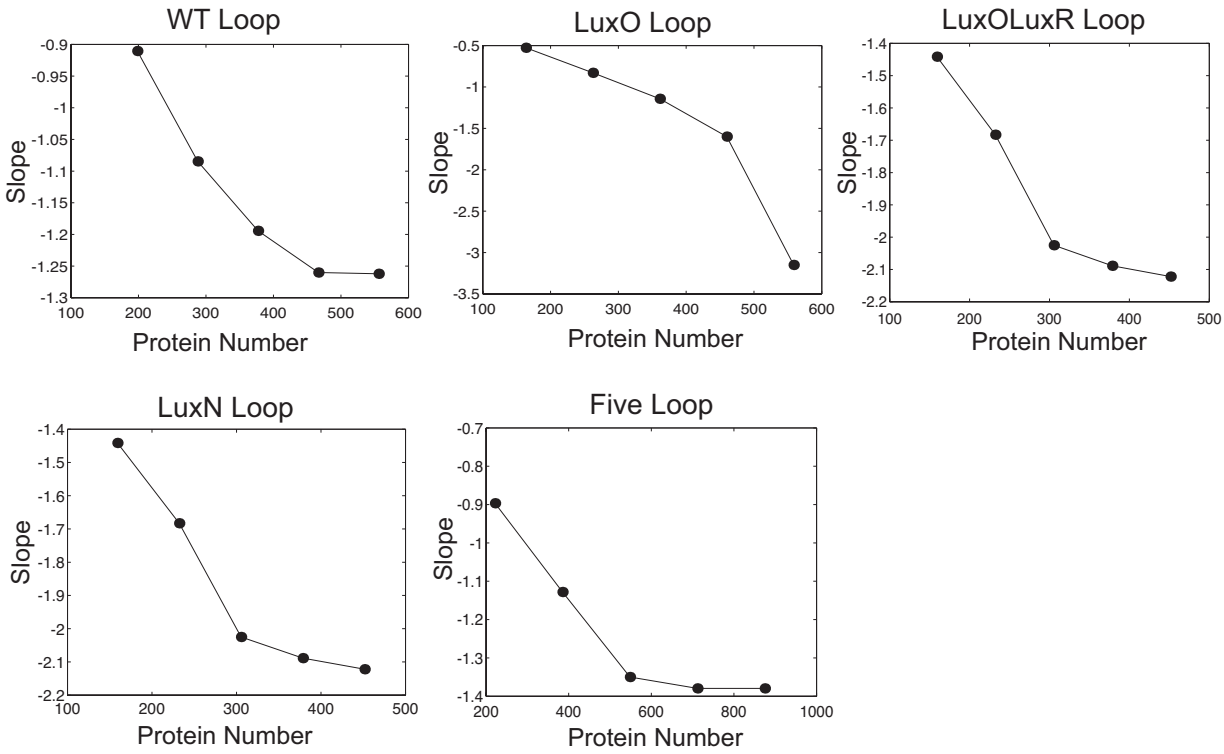

Figure S9. Slopes of constant LuxR-mCherry contours in the five *V. harveyi* strains. Slopes of mean LuxR contours were extracted from all strains using the input-output data shown in Figure 7. Plotted slopes are the slope of the straight line that best fits the constant-contour output level at each protein number. According to our mathematical model, the decrease in slope with increasing mean LuxR level reflects an increase in the ratio of LuxN to LuxPQ.

B. Mathematical Model

As discussed in the main text, many features of the dose-response data can be understood using a mathematical model for the *V. harveyi* quorum-sensing network. The model allows us to relate our results to those of Long et al. (Long et al., 2009) and extract the effective receptor ratio

directly from measured input-output contours. Finally, the model allows us to interpret how changing network architecture affects noise properties of the network.

B.1. Mathematical Model for Signal Integration

A mathematical model for the *V. harveyi* quorum-sensing circuit network was developed previously in (Long et al., 2009; Mehta et al., 2009). In those papers, the "open-loop" circuit without most feedback loops was modeled using a two-state model for receptors. This model explained the data well (Long et al., 2009) and allowed quantification of the effect of changing receptor ratios on information transmission (Mehta et al., 2009). This model will be used extensively in what follows and we summarize its major elements below.

B.1.1. Two-state Model for Receptors

Within the model, receptors exist in two states: a low kinase activity state we call "off" and a high kinase activity state, we call "on" (Keymer et al., 2006; Swem et al., 2008). Ligands, in our case autoinducers, act by binding to a receptor and changing the free energies and therefore the equilibrium between its two activity states. There are a total of four free-energy states with corresponding free energies: (i) on without ligand-bound E^{on}, (ii) on with ligand-bound $E^{on} - \log([\mathrm{L}]/K^{on})$, (iii) off without ligand-bound E^{off}, and (iv) off with ligand bound $E^{off} - \log([\mathrm{L}]/K^{off})$. In the absence of ligands, the receptors favor the on state, which implies $E^{on} < E^{off}$, but ligand binding favors the off state, which implies $K^{on} > K^{off}$. At equilibrium, the probability that a receptor is on is a function of the difference in free energies between the "on" states and the "off" states:

$$f = \varepsilon + \log\left(\frac{1 + [\mathrm{L}]/K^{off}}{1 + [\mathrm{L}]/K^{on}}\right), \qquad (1)$$

with $\varepsilon = E^{on} - E^{off}$, where all energies are expressed in units of the thermal energy $k_B T$. In particular, the equilibrium probability for a receptor to be on is

$$p_{on} = \frac{1}{1 + e^{f}}. \tag{2}$$

For K^{on} much larger than the typical ligand concentration and ε large and negative as observed for LuxN in the quorum-sensing network (Swem et al., 2008), the probability that a receptor is on becomes

$$\begin{aligned} p_{on} &= \frac{1}{1 + e^{\varepsilon}\left(\frac{1 + [\mathrm{L}]/K^{off}}{1 + [\mathrm{L}]/K^{on}}\right)} \\ &\approx \frac{1}{1 + \frac{[\mathrm{L}]}{K^{off} e^{-\varepsilon}}}. \end{aligned} \tag{3}$$

Defining a half-maximal inhibition constant $K_I = K^{off} e^{-\varepsilon}$, one finds the simple non-cooperative Hill function,

$$p_{on} \approx \frac{1}{1 + \frac{[\mathrm{L}]}{K_I}}. \tag{4}$$

B.1.2. Model for *V. harveyi* Quorum-sensing Phosphorelay

We denote the probabilities that LuxN and LuxPQ are in their on states by X and Y, respectively, with

$$X \approx \frac{1}{1 + \frac{[\mathrm{AI\text{-}1}]}{K_I^{\mathrm{AI\text{-}1}}}} \tag{5}$$

and

$$Y \approx \frac{1}{1 + \frac{[\text{AI-2}]}{K_I^{\text{AI-2}}}}. \tag{6}$$

Denote the total kinase activities in the on states of the two kinds of receptors by k_X and k_Y, respectively. Note, that by definition

$$k_X = N_X k_X^0 \tag{7}$$

$$k_Y = N_Y k_Y^0, \tag{8}$$

where N_X and N_Y are the number of LuxN and LuxPQ receptors, respectively and k_X^0 and k_Y^0 are the kinase activities of single LuxN and LuxPQ receptors in the on state, respectively. Furthermore, for notational simplicity and consistent with experiment, we assume that the kinase activity in the off state for both receptors is negligible. We also assume, based on experimental evidence, that the receptors have state-independent phosphatase activities. Denote the total phosphates activities of all LuxN and LuxPQ receptor by p_X and p_Y respectively, where,

$$p_X = N_X p_X^0 \tag{9}$$

$$p_Y = N_Y p_Y^0, \tag{10}$$

with p_X^0 and p_Y^0 the phosphatase activity of a single LuxN and LuxPQ receptor. The kinetics of the phosphorelay can be described by

$$\frac{d[\text{LuxU}\sim\text{P}]}{dt} = (k_X X + k_Y Y)([\text{LuxU}]_\text{T} - [\text{LuxU}\sim\text{P}]) - (p_X + p_Y + p_U)[\text{LuxU}\sim\text{P}]$$

$$-k_+[\text{LuxU}\sim\text{P}]([\text{LuxO}]_\text{T} - [\text{LuxO}\sim\text{P}]) + k_-[\text{LuxO}\sim\text{P}]([\text{LuxU}]_\text{T} - [\text{LuxU}\sim\text{P}]) \tag{11}$$

$$\frac{d[\text{LuxO}\sim\text{P}]}{dt} = k_+[\text{LuxU}\sim\text{P}]([\text{LuxO}]_\text{T} - [\text{LuxO}\sim\text{P}]) - k_-[\text{LuxO}\sim\text{P}]([\text{LuxU}]_\text{T} - [\text{LuxU}\sim\text{P}]),$$

where p_U is the spontaneous dephosphorylation rate for LuxU~P and $[\text{LuxU}]_\text{T}$ and $[\text{LuxO}]_\text{T}$ are the total concentrations of LuxU and LuxO proteins, respectively. We have neglected any background phosphorylation rate in the equations above for mathematical simplicity, but the qualitative results do not depend on this assumption in the biologically relevant limit where this rate is small. At steady state, we can set the left hand sides of these equations to zero yielding,

$$\frac{[\text{LuxU}\sim\text{P}]}{[\text{LuxU}]_\text{T}} = \frac{k_X X + k_Y Y}{k_x X + k_y Y + p_X + p_Y + p_U}. \tag{12}$$

A very similar expression can be derived for the fraction of phosphorylated LuxO, which we denote Z in the main text, by setting the left hand side of the bottom equation in (11) equal to zero and using (12). This yields

$$\frac{[\text{LuxO}\sim\text{P}]}{[\text{LuxO}]_\text{T}} = \frac{k_X X + k_Y Y}{k_x X + k_y Y + p} \tag{13}$$

with $p = \frac{k_-}{k_+}(p_X + p_Y + p_U)$. When the total dephosphorylation rate is large as observed in experiment (Long et al., 2009), we can approximate the above expression by

$$Z = \frac{[\text{LuxO}\sim\text{P}]}{[\text{LuxO}]_\text{T}} \approx \frac{k_X X + k_Y Y}{p} = \frac{k_+}{k_-}\frac{N_X k_X^0 X + N_Y k_Y^0 Y}{N_X p_X^0 + N_Y p_Y^0 + p_U}. \tag{14}$$

B.1.3. Modeling the Feedback Loops

A detailed kinetic model of the feedback loops in the system is currently impractical because of the large number of unknown parameters. In particular, modeling the interaction of the five sRNAs with multiple mRNA targets (LuxMN, LuxR, LuxO) is extremely sensitive to choices of parameters due to stoichiometric competition between mRNA targets (Levine et al., 2007; Mehta et al., 2008). For the

present, we choose to ignore the details of the internal feedback loops and instead make a simple phenomenological model. In particular, we model the number of LuxR proteins as some monotonically decreasing function, $R(Z)$, of the fraction of phosphorylated LuxO proteins,

$$[\text{LuxR}] = R(Z), \tag{15}$$

with Z given by (14). We make no assumption about the specific form of $R(Z)$. The effect of the feedback on LuxN is explicitly incorporated by making the number of LuxN receptors a function of the LuxO~P level, $N_X = N_X(Z)$. Given a model of the feedback, $N_X(Z)$, one can explicitly solve (14) for Z.

B.2. Comparing Data to Long et al.

Expression (14) is a general result for the fraction of phosphorylated LuxO set by the *V. harveyi* phosphorelay. Dose-response experiments performed in (Long et al., 2009) using GFP as a reporter of LuxO~P activity suggest that the circuit tunes receptor ratios so that $k_X \approx k_Y$ ($N_X k_X^0 = N_Y k_Y^0$) in expression (14). In the strains used in (Long et al., 2009), GFP was put under the control of the strongest quorum sensing sRNA promoter, *Pqrr*4, and the master transcriptional regulator LuxR was deleted. The mean GFP levels were well-fit by a function of the form (Long et al., 2009)

$$\text{GFP} = \text{GFP}_0 + \frac{1.53}{1 + \frac{[\text{AI-1}]}{6.9\text{nM}}} + \frac{1.49}{1 + \frac{[\text{AI-2}]}{6.4\text{nM}}}. \tag{16}$$

As pointed out in by (Long et al., 2009), this expression is of the form (14) with $\frac{k_X}{p} = 1.53$, $\frac{k_Y}{p} = 1.49$, and the constants $K_I^{\text{AI-1}}$ and $K_I^{\text{AI-2}}$ appearing in the receptor probabilities, (5) and (6), given by $K_I^{\text{AI-1}} = 6.9\text{nM}$ and $K_I^{\text{AI-2}} = 6.4\text{nM}$, yielding

$$\text{GFP} = \text{GFP}_0 + 1.53\,X + 1.49\,Y. \tag{17}$$

Thus, the constant output contours of GFP, and presumably of LuxO~P, as functions of X and Y are just straight lines with slopes approximately -1.

B.3. Feedback Loops and Noise

In these section, we show that the mathematical model (14) explains many of the noise properties seen in the data. It is now well established that negative feedbacks reduce noise, defined as the ratio of the standard deviation to mean of a protein. The underlying reason for this is that any stochastic increase in the output reduces the input signal, and hence leads to a subsequent decrease in the output. In contrast, positive feedback loops generally lead to an increase in noise because a fluctuation due to an increased output signal results in an increase in the input signal. We use these general facts to explore how the negative feedback on LuxN affects the noise properties of the circuit.

The sign of a feedback can be calculated by measuring the open-loop gain. The open-loop gain is the gain of a circuit where all the feedbacks have been broken. In particular, since the the LuxN feedback is a function of phospho-LuxO levels via sRNAs, the relevant open-loop gain, g_{open}, is simply the change in LuxO~P protein number in response to small change in the number of LuxN receptors,

$$g_{open} = \frac{\partial Z}{\partial N_X}. \tag{18}$$

Since increasing Z decreases LuxN via negative regulation by small RNAs, the feedback loop acts as a negative feedback loop when $g_{open} > 0$ and as a positive feedback loop when $g_{open} < 0$. The LuxR protein levels simply serve in this scenario as a readout for the fluctuations in phospho-LuxO numbers. From (14), one has

$$\frac{\partial Z}{\partial N_X} = \frac{1}{p}\left(k_X^0 X - \frac{k_-}{k_+} p_X^0 Z\right). \tag{19}$$

Thus, when

$$\frac{X}{Z} > \frac{p_X^0 k_-}{k_X^0 k_+}, \tag{20}$$

the feedback is negative, whereas for

$$\frac{X}{Z} < \frac{p_X^0 k_-}{k_X^0 k_+}, \tag{21}$$

the feedback is positive.

Experimentally, the noise in the system is large at low AI-2 concentrations where Z takes on intermediate to high values. Thus, the equations above imply that for small X (high AI-1 concentrations), the LuxN feedback loop acts as a positive feedback that amplifies noise whereas for large X (low AI-1 concentrations), the feedback loop is negative. This is consistent with the data and the discussion in the main text.

C.

Table SI. *V. harveyi* strains and plasmids used in this study.

Strain	**Relevant genotype**	**Reference**
TL27	Δ*luxM,* Δ*luxS,* Δ*cqsS*	(Long et al., 2009)
KT833	Δ*luxM,* Δ*luxS,* Δ*cqsS, luxR-mCherry*	(Tu et al., 2010)
TL112	Δ*luxM,* Δ*luxS,* Δ*cqsS, luxR-mCherry,* P_{tac}-*gfp*	(Long et al., 2009)
ST038	Δ*luxM,* Δ*luxS,* Δ*cqsS, luxR-mCherry,* P_{cmw275}-*gfp*	This study
ST055	Δ*luxM,* Δ*luxS,* Δ*cqsS,* P_{cmw275}-*gfp*	This study
KT641	Δ*luxM,* Δ*luxS,* Δ*cqsS,* LuxO Loop	(Tu et al., 2010)
KT836	Δ*luxM,* Δ*luxS,* Δ*cqsS,* LuxO Loop, *luxR-mCherry*	(Tu et al., 2010)
ST053	Δ*luxM,* Δ*luxS,* Δ*cqsS,* LuxO Loop, LuxR Loop, *luxR-mCherry*	This study
JS492	Δ*luxM,* Δ*luxS,* Δ*cqsS,* LuxN Loop, *luxR-mCherry*	This study

JS489	Δ*luxM,* Δ*luxS,* Δ*cqsS,* LuxO Loop, LuxR Loop, LuxN Loop, *luxR-mCherry*	This study
ST165	Δ*luxM,* Δ*luxS,* Δ*cqsS,* Δ*luxN, luxR-mCherry,* LuxN on, Kan^r	This study
ST168	Δ*luxM,* Δ*luxS,* Δ*cqsS,* Δ*luxN,* LuxO Loop*, luxR-mCherry,* LuxN-on, Kan^r	This study
ST174	Δ*luxM,* Δ*luxS,* Δ*cqsS,* Δ*luxN, luxR-mCherry,* empty vector, Kan^r	This study
JS460	scar-*luxMN*	This study
JS466	Δ*qrr1*-5, scar-*luxMN*	This study
JS464	$luxO^{D47E}$*-CmR,* scar-*luxMN*	This study
JS469	BP^- *luxMN*	This study
JS475	Δ*qrr1*-5, BP^- *luxMN*	This study
JS473	$luxO^{D47E}$*-CmR,* BP^- *luxMN*	This study
JS104	*luxMN-FLAG*	This study
JS200	Δ*qrr1*-5, *luxMN-FLAG*	This study
JS108	$luxO^{D47E}$*-CmR, luxMN-FLAG*	This study
STR0018	MC4100 λatt-$QrrLoop^-$-$LuxO^{D47E}$	This study
BB170	*luxN::*Tn5KanR	(Bassler et al., 1993)
TL25	Δ*luxM* Δ*luxPQ* Δ*cqsS*	(Long et al, 2009)
KM387	Δ*luxS*	(Henke and Bassler, 2004)
Strain	**Relevant genotype**	**Reference**
pKM1556	pLAFR2 with Δ*luxM*, Tet^r	(Mok et al., 2003)
pJS1410	p KM1556 with BP^--Kan^r, Tet^r	This study
pST153	pKM1556 with Δ*luxN*::Cm^r, Tet^r	This study
pST157	pJV025 with IPTG and Theophyline inducible LuxN, Kan^r	This study
pJS1239	*luxM-gfp*, Kan^r	This study
pJS1427	BP^-*-luxM-gfp*, Kan^r	This study
pKT1679	*luxM-gfp*, Cm^r	This study
pJS1151	BP^-*-luxM-gfp*, Cm^r	This study
pKT1073	pLAFR-Δ*qrr4*, Tet^r	This study

pJS1384	pLAFR-*kan*^{r}-*qrr4*, Tet^{r}	This study
pJS1388	pLAFR-*kan*^{r}-*BP*$^{-}$-*qrr4*	This study

D. References

Bassler BL, Wright M, Showalter RE, Silverman MR. (1993). Intercellular signaling in *Vibrio harveyi*: sequence and function of genes regulating expression of luminescence. Mol Micriobol. *9,* 773-786.

Freeman JA, Lilley BN, Bassler BL. (2000). A genetic analysis of the fuctions of LuxN; a two-component hybrid sensor kinase that regulates quorum sensing in *Vibrio harveyi*. Mol Microbiol. *35,* 39-49.

Henke JM and Bassler BL. (2004). Three Parallel Quorum-Sensing Systems Regulate Gene Expression in *Vibrio harveyi*. J. Bacteriol. *186,* 6902-6914.

Keymer, J.E., Endres, R.G., Skoge, M., Meir, Y., and Wingreen, N.S. (2006). Chemosensing in Escherichia coli: Two regimes of two-state receptors. Proc. Natl. Acad. Sci. U. S. A. *103,* 1786-1791.

Levine, E., Zhang, Z., Kuhlman, T., and Hwa, T. (2007). Quantitative characteristics of gene regulation by small RNA. PloS Biology *5,* 1998-2010.

Long, T., Tu, K.C., Wang, Y., Mehta, P., Ong, N.P., Bassler, B.L., and Wingreen, N.S. (2009). Quantifying the Integration of Quorum-Sensing Signals with Single-Cell Resolution. PLoS Biology *7,* e68 OP.

Mehta, P., Goyal, S., Long, T., Bassler, B.L., and Wingreen, N.S. (2009). Information processing and signal integration in bacterial quorum sensing. Molecular Systems Biology *5,* 325.

Mehta, P., Goyal, S., and Wingreen, N.S. (2008). A quantitative comparison of sRNA-based and protein-based gene regulation. Molecular Systems Biology *4,* 221.

Swem, L.R., Swem, D.L., Wingreen, N.S., and Bassler, B.L. (2008). Deducing receptor signaling parameters from in vivo analysis: LuxN/AI-1 quorum sensing in *Vibrio harveyi*. Cell *134,* 461-473.

Tu, K.C., Long, T., Svenningsen, S.L., Wingreen, N.S., and Bassler, B.L. (2010). Negative Feedback Loops Involving Small Regulatory RNAs Precisely Control the *Vibrio harveyi* Quorum-Sensing Response. Mol. Cell *37,* 567-579.